
AFRL-AFOSR-VA-TR-2018-0383

# Observations with the 1.6 Meter New Solar Telescope in Big Bear: Origins of Space Weather

**Philip Goode**
**NEW JERSEY INST OF TECH NEWARK**

**10/09/2018**
**Final Report**



Air Force Research Laboratory
AF Office Of Scientific Research (AFOSR)/ RTB1
Arlington, Virginia 22203
Air Force Materiel Command

# REPORT DOCUMENTATION PAGE

*Form Approved*
*OMB No. 0704-0188*



| 1. REPORT DATE *(DD-MM-YYYY)* | 2. REPORT TYPE | 3. DATES COVERED *(From - To)* |
|---|---|---|
| 05-09-2018 | Final | 15-09-2018-14-09-2018 |

**4. TITLE AND SUBTITLE**

Observations with the 1.6 Meter New Solar Telescope in Big Bear: Origins of Space Weather

**5a. CONTRACT NUMBER**

**5b. GRANT NUMBER**

AFOSR FA9550-15-1-0322

**5c. PROGRAM ELEMENT NUMBER**

**6. AUTHOR(S)**

Goode, Philip R.
Yurchyshyn, Vasyl B.
Cao, Wenda

**5d. PROJECT NUMBER**

**5e. TASK NUMBER**

**5f. WORK UNIT NUMBER**

**7. PERFORMING ORGANIZATION NAME(S) AND ADDRESS(ES)**

New Jersey Institute of Technology
University Heights
Newark, New Jersey 07102

**8. PERFORMING ORGANIZATION REPORT NUMBER**

**9. SPONSORING/MONITORING AGENCY NAME(S) AND ADDRESS(ES)**

Air Force Office of Scientific Research, AFOSR/RTB
875 North Randolph Street, Room 3112
Arlington, VA 22203-1954

**10. SPONSOR/MONITOR'S ACRONYM(S)**

AFOSR/PKR2

**11. SPONSOR/MONITOR'S REPORT NUMBER(S)**

**12. DISTRIBUTION/AVAILABILITY STATEMENT**

Publically Available (UU)

**13. SUPPLEMENTARY NOTES**

None

**14. ABSTRACT**

Here we summarize principal results of our AFOSR supported research efforts. We have designed, build and implemented the first solar multi-conjugate adaptive optics (MCAO) system called Clear, which is the most unique generation of adaptive optics in Big Bear that is the latest fruit from a nearly two decade long collaboration between BBSO and the National Solar Observatory. Clear has three DMs conjugated to the ground, 3 km and 8 km respectively, to correct all turbulence in the field of view from the ground to 11 km above ground. The conjugation altitudes can be quickly changed if seeing changes.

**15. SUBJECT TERMS**

Basic Research, space sciences, solar physics

| 16. SECURITY CLASSIFICATION OF: | | | 17. LIMITATION OF ABSTRACT | 18. NUMBER OF PAGES | 19a. NAME OF RESPONSIBLE PERSON |
|---|---|---|---|---|---|
| a. REPORT | b. ABSTRACT | c. THIS PAGE | | | Goode, Philip R. |
| UU | UU | UU | UU | 15 | 19b. TELEPHONE NUMBER *(Include area code)* 908-249-1943 |

# Final Report

*AFOSR Project: FA9550-15-1-0322 Start Date 9/14/2015*

*PI: Philip Goode*

## *1. Instrumental Work and Research Highlights*

On Sept 14, 2015, our current three-year AFOSR FA9550-15-1-0322 grant (Goode, PI) started, which has primarily supported Vasyl Yurchyshyn who performs data collection, processing, analysis, and interpretation yielding new scientific results. Our success is built on prior AFOSR support for science using the Goode Solar Telescope (GST, formerly New Solar Telescope), as well as earlier support for GST instrumentation fed using light corrected by successive generations of adaptive optics (AO) on which Goode took the lead.

Under current AFOSR support, the GST was used to observe the photosphere, chromosphere and up to the transition region with unprecedented resolution to elucidate the fundamental nature of the dynamics of solar magnetism and its evolution. We use the GST in sustained campaigns, which has been at the core of BBSO's ability to provide unique data in support of the community's efforts to understand our star and its environs. Observing campaigns are essential to determine the origin of "space weather", which arises from solar magnetic storms and can have deleterious effects on satellites, as well as the terrestrial power grid, telecommunications, and other aspects of human civilization.

Data requests come to BBSO on a daily basis from around the world. The GST generates far more data than the old BBSO telescope. This has presented a more challenging problem for archiving and community access. To facilitate broader use of GST data, all the data are placed online in a user friendly way. Users of GST data are only asked to acknowledge BBSO in their resulting publications.

### *1.1 Principal MCAO Progress: Clear Widens the Field for Observations of the Sun*

The stunning successes of solar adaptive optics (AO) have come from systems with a single deformable mirror (DM) in which only the isoplanatic patch (typically $\leq 10''$ in visible light under good seeing conditions) can be corrected to the diffraction limit with decreasing correction as distance from the patch increases. A multi-conjugate AO (MCAO) setup has two, or more, DMs to correct anisoplanatism with each DM being conjugated to a different layer of atmospheric turbulence. BBSO *Clear* (Schmidt et al., 2017) is the first solar MCAO system to significantly improve (triple) the corrected FOV and continues a nearly two decade long collaboration between BBSO and the National Solar Observatory (NSO) in adaptive optics. *Clear* has three DMs conjugated to the ground, 3 km and 8 km respectively, to correct all turbulence in the field of view from the ground to 11 km above ground. The conjugation altitudes can be quickly changed if seeing changes.

This is technically difficult, but wide-field, diffraction-limited correction is the holy grail for addressing the fundamental dynamics of our star and origin of space weather, and must be done. We have enjoyed noteworthy successes. Our motivation to build such a challenging system comes from the fact that the GST is the only solar telescope in the U.S. having sufficient aperture and modulation transfer function to resolve what is generally regarded as the fundamental scale of the Sun's surface.

It is important to bear in mind that magnetic field dynamics are the cause of the Sun's powerful, explosive and non-local events, like flaring and coronal mass ejections (CMEs), which can cover upwards of ~50 $''$ and occasionally more. We have studied several such events and every time important details of flare evolution were absent due to inferior resolution outside the isoplanatic patch (see references below).

Results from the first ever clearly and easily visible successful solar MCAO imaging system are

shown in Fig. 1 (Schmidt et al., 2017), where each panel 2 is a superposition of 150 MCAO, GLAO, and CAO frames used without any post-processing of the images.

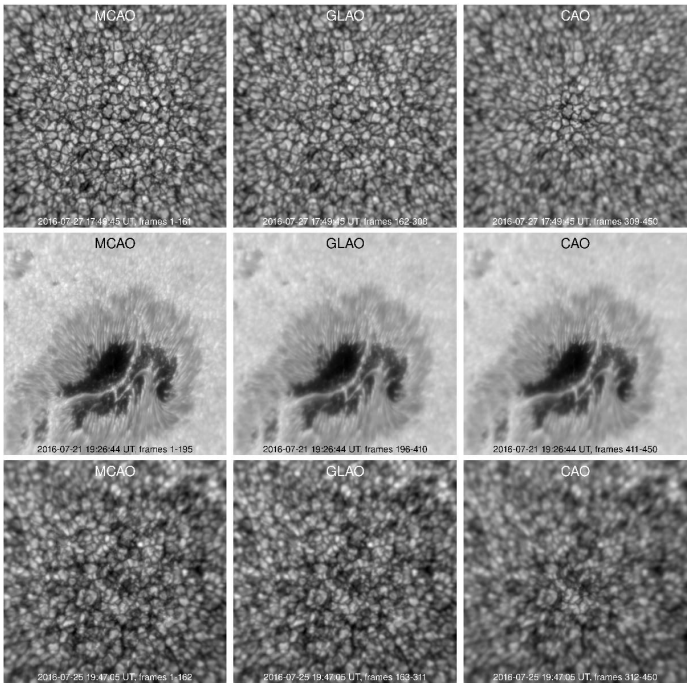


*Fig. 1 — Each image is the sum of a burst of ~150 exposures taken over about 10 seconds. Each row shows nearly simultaneous images. Top Row: Taken of granulation at 710 nm. The trebling of the corrected field is apparent. Middle Row: An active region with light bridge. Fine structure is apparent. Bottom Row: Granulation in G-band (405 nm) light, which is at the bluest end of the visible spectrum.*

In the upper left panel of Fig. 1, the great improvement is obvious with < 0 ″ .2 intergranular lane bright points (Goode et al., 2010) being easily apparent (see insets) even at the edge of the ~35″ corrected FOV − the setup that was aimed for a 35″ corrected FOV and it was achieved. In the lower left panel, the fibril structure of the umbra and penumbra look clear, as is the granular field compared to GLAO and CAO results (compare insets). Images like those in Fig. 1 were seen many times during the ten day observing run near the end of July 2016 and three runs in Summer of 2017. Another way to understand Fig. 1 is to consider the generalized Fried parameter (Cagigal & Canales, 2000), which is a measure of the Fried parameter across the field and can be computed using the KISIP image reconstruction software (W ¨oger et al., 2008), which indicates a full correction of entire field by MCAO. It is noteworthy that this was achieved on a granular field, which makes the MCAO performance even more impressive because it is harder to lock and keep any AO system locked on the relatively low-contrast granulation compared to the rather high-contrast features like pores. The rightmost panels of Fig. 1 show superposed images gained with CAO correction. Relatively small isoplanatic patches are apparent in the right panels with correction concentrated near the center of the FOV. One can see advantages for using either CAO or GLAO depending on the requirements of the observations with CAO providing better image detail in a small FOV, while the single DM GLAO performance resulted in a lower but more homogeneous image detail over the field compared to CAO correction. CAO and GLAO are regular instruments on the GST an observers can instantaneously switch between them.

1.2 *Principal Science Results from Current AFOSR Support*

Here we summarize principal results of our AFOSR supported research efforts. We have designed, build and implemented the first solar multi-conjugate adaptive optics (MCAO) system called Clear (Schmidt et al., 2017), which is the most unique generation of adaptive optics in Big Bear that is the latest fruit from a nearly two decade long collaboration between BBSO and the National Solar Observatory. Clear has three DMs conjugated to the ground, 3 km and 8 km respectively, to correct all turbulence in the field of view from the ground to 11 km above ground. The conjugation altitudes can be quickly changed if seeing changes. The new system significantly improves (triples) the corrected FOV thus allowing us to address the fundamental dynamics of our star and origin of space weather. Clear is the first solar MCAO to

correct a wide enough field to cover an entire active region, which is essential for studies of space weather.

On the smallest end of the studied spatial range using GST data, we found that an eruptive X1.6 flare on 7 November 2015 was directly triggered by a small-scale flux emergence that occurred inside a δ-sunspot. We also found that flux emergence and magnetic reconnection frequently occur on light bridges inside sunspots, which should be properly accounted for in future modeling efforts of sunspots. Our studies showed that emerging fields are highly twisted and their emergence is associated with repeated flares and reconnections that enable the transport of that twist and energy into the solar corona thus forming erupting magnetic flux tubes.

In the midrange of scales, the emergence of active regions (ARs) was found to follow two different pathways, rapid and gradual emergence. Further analysis is needed to understand how their emergence rate is reflected in flaring activity, which may lead to the development of flare forecasting tools. Evolution of ARs was further scrutinized using data-driven numerical magnetohydrodynamic (MHD) modeling and observations. We were able to explain why one of the strongest ARs produced no coronal mass ejections. Our studies also showed that although eruptions may be triggered by small-scale events they are a global phenomena that often involve volumes exceeding that of a relevant AR and producing global post eruption loops and circular flare ribbons.

Our studies of solar activity on largest temporal and spatial scales showed that most of the eruptions occurs in a large and complex ARs of classes D, E, and F. The monthly mean maximum CME speed index (MCMESI) correlates well with monthly mean ionospheric critical frequencies foF1 and foF2, which are the highest magnitude of frequency above which the waves penetrates the ionosphere and below which the waves are reflected back from the ionosphere. Their values are not fixed depend upon electron density of ionosphere. The major contributors to the solar mean magnetic field (SMMF) were found to be strong and moderate magnetic fields in contrast to the earlier view that the weakest fields contribute the most. Our efforts to predict future level of solar activity resulted in the prediction of a weak future solar cycle 25 with the peak sunspot number being about 150 that is expected to occur early in 2023.

### *2. List of Publications Supported by the AFOSR Grant*


1. *Prediction of solar cycle 25: a non-linear approach*, Sarp, V., Kilcik, A., Yurchyshyn, V., Rozelot, J.P., Ozguc, A., 2018, MNRAS, 481, 2981
2. *The evolution of flaring and non-flaring active regions,* Kilcik, A., Yurchyshyn, V., Sahin, S., Sarp, V., Obridko, V., Ozguc, A., Rozelot, J.P., 2018, MNRAS, 477, 293
3. *Signature of a possible relationship between the maximum CME speed index and the critical frequencies of the F1 and F2 ionospheric layers: Data analysis for a mid-latitude ionospheric station during the solar cycles 23 and 24*, Kilcik, A., Ozguc, A., Yiğit, E., Yurchyshyn V., Donmez, B., 2018, J. Atm. Sol-Ter. Phys., 171, 131
4. *Temporal and Periodic Variations of Sunspot Counts in Flaring and Non-Flaring Active Regions*, Kilcik, A., Yurchyshyn, V., Donmez, B., Obridko, V. N., Ozguc, A., Rozelot, J.P., 2018, Sol. Phys., 293, 63
5. *Frequently Occurring Reconnection Jets from Sunspot Light Bridges*, Tian, H., Yurchyshyn, V., Peter, H., Solanki, S. K., Young, P. R., Ni, L., and 9 co-authors, 2018, Astrophys. J., 854, 92
6. *Observation of a Large-scale Quasi-circular Secondary Ribbon Associated with Successive Flares and a Halo CME,* Lim, E-K., Yurchyshyn, V., Kumar, P., Cho, K., Jiang, C., Kim, S. and 4 co-authors, 2017, Astrophys. J., 850/2, article id. 167
7. *Contribution to the Solar Mean Magnetic Field from Different Solar Regions,* Kutsenko, A.S., Abramenko, V. I., and Yurchyshyn, V. B., 2017, Sol. Phys., 292, 121, 10.1007/s11207-017-1145-9

8. *Clear Widens the Field for Observations of the Sun with Multi-conjugate Adaptive Optics*, Schmidt, D., Gorceix, N., Goode, P.R., Marino, J., Rimmele, T., Berkefeld, T., Woger, F., Zhang, X., Rigaut, F., van der Luhe, O., 2017, A&A, 597, L8
9. *How Did a Major Confined Flare Occur in Super Solar Active Region 12192?*, Jiang, C. W., Wu, S. T., Yurchyshyn, V., Wang, H., Feng, X. S., Hu, Q., 2016, Astrophys. J., 828, 62
10. *Multi-wavelength observations of a flux rope formation by series of magnetic reconnection in the chromosphere*, Kumar, P., Yurchyshyn, V., Cho, K.S., Wang, H., 2017, A&A, 603, id.A36
11. *High-resolution Observations of a White-light Flare with NST*, Yurchyshyn, V., Kumar, P., Abramenko, V., et al., 2017, Astrophys. J., 838, 32
12. *Chromospheric Plasma Ejections in a Light Bridge of a Sunspot*, Song, D., Chae, J., Yurchyshyn, V., et al., 2017, Astroph. J.,835, 240
13. *Impact of the Icme-Earth Geometry on the Strength of the Associated Geomagnetic Storm: The September 2014 and March 2015 Events*, Cho, K.-S., Marubashi, K., Kim, R.-S., Park, S.-H., Lim, E.-K., Kim, S.-J., Kumar, P., Yurchyshyn, V., Moon, Y.-J., Lee, J.-O., 2017, J. Korea Astron. Soc., 50, 29
14. *Analysis of the Flux Growth Rate in Emerging Active Regions on the Sun*, Abramenko, V. I. , Kutsenko, A. S., Tikhonova, O. I., & Yurchyshyn, V. B., 2017, Sol. Phys., 292,article id.48
15. *Solar and Geomagnetic Activity Relation for the Last two Solar Cycles*, Kilcik, A., Yigit, E., Yurchyshyn, V., Ozguc, A., & Rozelot, J.P., 2017, Sun & Geosphere, 12, 1, 31-39
16. *Flare-production potential associated with different sunspot groups*, Eren, S., Kilcik, A., Atay, T., Miteva, R., Yurchyshyn, V., Rozelot, J. P., Ozguc, A., 2017, MNRAS, 465, 68-75
17. *Multiwavelength Observations of a Slow-rise, Multistep X1.6 Flare and the Associated Eruption,* Yurchyshyn, V., Kumar, P., Cho, K.-S., Lim, E.-K., Abramenko, V. I., 2015, Astrophys. J., 812/2, article.id. 172
18. *Observations of a Series of Flares and Associated Jet-like Eruptions Driven by the Emergence of Twisted Magnetic Fields,* Lim, E-K., Yurchyshyn, V., Park, S-H., Kim, S., Cho, K-S., Kumar, P., Chae, J., Yang, H., Cho, K., Song, D., Kim, Y-H., 2016, Astrophys. J., 817/1, article.id. 39
19. Formation and Eruption of a Small Flux Rope in the Chromosphere Observed by NST, IRIS, and SDO by P. Kumar, V. Yurchyshyn, H. Wang, & K.S. Cho, 2015, Astrophys. J., 809/1, article id. 83

### *3. Instrumental Work and Research Update*

**Clear widens the field for observations of the Sun with multi-conjugate adaptive optics**, Schmidt, D., Gorceix, N., Goode, P. R., Marino, J., Rimmele, T., Berkefeld, T., Wöger, F., Zhang, X., Rigaut, F., von der Lühe, O., 2017, A&A, 597, L8

The multi-conjugate adaptive optics (MCAO) pathfinder Clear on the New Solar Telescope in Big Bear Lake has provided the first-ever MCAO-corrected observations of the Sun that show a clearly and visibly widened corrected field of view compared to quasi-simultaneous observations with classical adaptive optics (CAO) correction. Clear simultaneously uses three deformable mirrors, each conjugated to a different altitude, to compensate for atmospheric turbulence. While the MCAO correction was most effective over an angle that is approximately three times wider than the angle that was corrected by CAO, the full 53" field of view did benefit from MCAO correction. We further demonstrated that ground-layer-only correction is attractive for solar observations as a complementary flavor of adaptive optics for observational programs that require homogenous seeing improvement over a wide field rather than diffraction-limited resolution. We show illustrative images of solar granulation and of a sunspot obtained on different days in July 2016, and present a brief quantitative analysis of the generalized Fried parameters of the images.

The BBSO MCAO system, Clear, uses three deformable mirrors (DMs) each with a different depth of field and conjugation altitude so that there is full correction covering from the ground to about 11 km. Clear uses nine guide regions (solar counterpart to nighttime guide stars). GLAO and CAO use a single DM, but GLAO uses a wide field correction. CAO and GLAO are in regular operation at BBSO,

but MCAO is still in testing phase.

**High-resolution Observations of a White-light Flare with NST**, *Yurchyshyn, V., Kumar, P., Abramenko, V., et al.,* 2017, Astrophys. J., 838, 32

Using high-resolution data from the New Solar Telescope, we studied fine spatial and temporal details of an M1.3 white-light (WL) flare, which was one of three homologous solar flares (C6.8, M1.3, and M2.3) observed in close proximity to the west solar limb on 2014 October 29 in NOAA active region 12192. We report that the TiO WL flare consists of compact and intense cores surrounded by less intense spatial halos. The strong and compact WL cores were measured to be ≈ 0.2 Mm across, with an area of about $10^{14}$ cm$^2$. Several TiO features were not co-spatial with Hα flare ribbons and were displaced toward the disk center by about 500 km, which suggests that the TiO and Hα radiation probably did not originate in the same chromospheric volume. The observed TiO intensity enhancements are not normally distributed and are structured by the magnetic field of the penumbra.

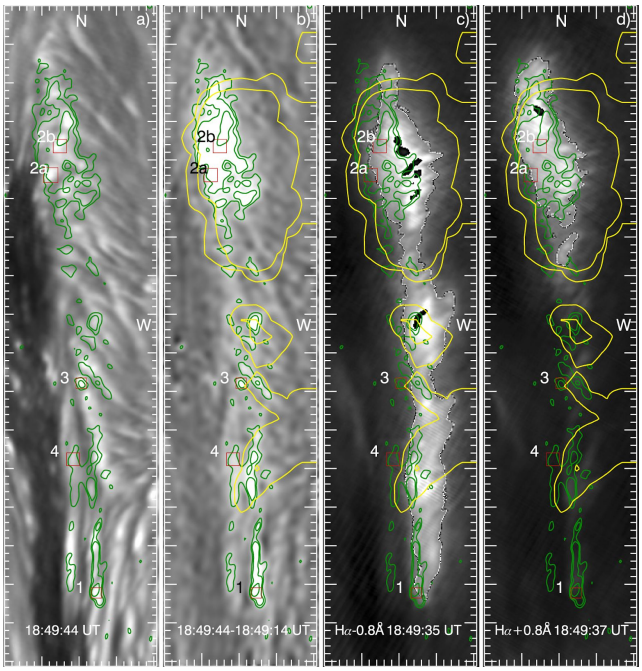


*Fig. 4. — M1.3 WL flare as seen at the HXR peak time with TiO 7057Å (panel (a)) and Hα filters (panels (c) and (d)). Panel (b) is a TiO difference image (18:49:44–18:49:14 UT). The green contours plotted in all panels outline TiO intensity enhancements at 6%, 10%, and 22% levels of the QS intensity. The red boxes outline areas where the intensity profiles were determined. The yellow contours outline AIA 94 Å emission. Note that the south (lower) half of the Hα+0.8 Å ribbon (panel (d)) is not seen here, as it was obscured by unrelated jets occurring in the foreground. The large tick interval is 1 Mm. The dark patches inside the flare ribbon (panels (c) and (d)) represent saturated pixels.*

**Chromospheric Plasma Ejections in a Light Bridge of a Sunspot,** *Song, D., Chae, J., Yurchyshyn, V., et al.,* 2017, Astrophys. J., , 835, 240

Light bridges (LBs) inside a sunspot produce small-scale plasma ejections and transient brightenings in the chromosphere, but the nature and origin of such phenomena are still unclear. Utilizing the high-spatial and high-temporal resolution spectral data taken with the Fast Imaging Solar Spectrograph and the TiO 7057 Å broadband filter images installed at the 1.6 m New Solar Telescope of Big Bear Solar Observatory, we report arcsecond-scale chromospheric plasma ejections (1.″7) inside a LB. Interestingly, the ejections are found to be a manifestation of upwardly propagating shock waves as evidenced by the saw-tooth patterns seen in the temporal-spectral plots of the Ca ii 8542 Å and Hα intensities. We also found a fine-scale photospheric pattern (1″) diverging with a speed of about 2 km s$^{-1}$ two minutes before the plasma ejections, which seems to be a manifestation of magnetic flux emergence. As a response to the plasma ejections, the corona displayed small-scale transient brightenings. Based on our findings, we suggest that the shock waves can be excited by the local disturbance caused by magnetic reconnection between the emerging flux inside the LB and the adjacent umbral magnetic field. The disturbance generates slow-mode waves, which soon develop into shock waves, and manifest themselves as the

arcsecond-scale plasma ejections. It also appears that the dissipation of mechanical energy in the shock waves can heat the local corona.

**Frequently Occurring Reconnection Jets from Sunspot Light Bridges**, Tian, H., Yurchyshyn, V., Peter, H., Solanki, S. K., Young, P. R., Ni, L., and 9 co-authors, 2018, 2018, Astrophys. J., 854, 92

Solid evidence of magnetic reconnection is rarely reported within sunspots, the darkest regions with the strongest magnetic fields and lowest temperatures in the solar atmosphere. Using the world's largest solar telescope, the 1.6 m Goode Solar Telescope, we detect prevalent reconnection through frequently occurring fine-scale jets in the Hα line wings at light bridges, the bright lanes that may divide the dark sunspot core into multiple parts. Many jets have an inverted Y-shape, shown by models to be typical of reconnection in a unipolar field environment. Simultaneous spectral imaging data from the Interface Region Imaging Spectrograph show that the reconnection drives bidirectional flows up to 200 km $s^{-1}$, and that the weakly ionized plasma is heated by at least an order of magnitude up to 80,000 K. Such highly dynamic reconnection jets and efficient heating should be properly accounted for in future modeling efforts of sunspots. Our observations also reveal that the surge-like activity previously reported above light bridges in some chromospheric passbands such as the Hα core has two components: the ever-present short surges likely to be related to the upward leakage of magnetoacoustic waves from the photosphere, and the occasionally occurring long and fast surges that are obviously caused by the intermittent reconnection jets.

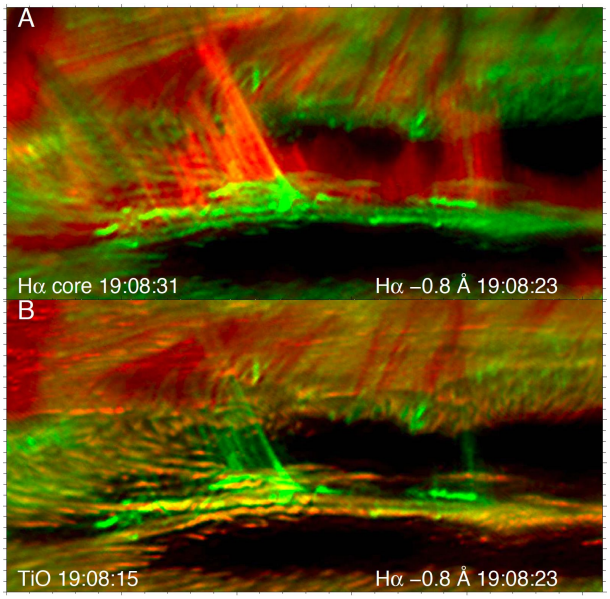


**Observation of a Large-scale Quasi-circular Secondary Ribbon Associated with Successive Flares and a Halo CME**, Lim, E-K., Yurchyshyn, V., Kumar, P., Cho, K., Jiang, C., Kim, S., Yang, H., Chae, J., Cho, K-S., Lee, J., 2017, Astrophys. J., 850/2, article id. 167

Solar flare ribbons provide an important clue to the magnetic reconnection process and associated magnetic field topology in the solar corona. We detected a large-scale secondary flare ribbon of a circular shape that developed in association with two successive M-class flares and one coronal mass ejection. Using multi-wavelength data from Solar Dynamics Observatory, RHESSI, XRT, and Nobeyama, along with magnetic field extrapolations, we found that: (1) the secondary ribbon location is consistent with those of the field line footpoints of a fan-shaped magnetic structure that connects the flaring region and the ambient decaying field; (2) the second M2.6 flare occurred when the expanding coronal loops driven by the first M2.0 flare encountered the background decayed field; (3) immediately after the second flare, the secondary ribbon developed along with dimming regions. Based on our findings, we suggest that interaction between the expanding sigmoid field and the overlying fan-shaped field triggered the secondary reconnection that resulted in the field opening and formation of the quasi-circular secondary ribbon. We thus conclude that interaction between the AR and the ambient large-scale fields should be taken into account to fully understand the entire eruption process.

**How Did a Major Confined Flare Occur in Super Solar Active Region 12192?,** *Jiang, C. W., Wu, S. T., Yurchyshyn, V., Wang, H., Feng, X. S., Hu, Q.,* 2016, Astrophys. J., 828, 62

We studied the physical mechanism of a major X-class solar flare that occurred in the super NOAA active region (AR) 12192 using data-driven numerical magnetohydrodynamic (MHD) modeling complemented with observations. With the evolving magnetic fields observed at the solar surface as bottom boundary input, we drive an MHD system to evolve self-consistently in correspondence with the realistic coronal evolution. During a two-day time interval, the modeled coronal field has been slowly stressed by the photospheric field evolution, which gradually created a large-scale coronal current sheet, i.e., a narrow layer with intense current, in the core of the AR. The current layer was successively enhanced until it became so thin that a tether-cutting reconnection between the sheared magnetic arcades had set in, which led to a flare. The modeled reconnecting field lines and their footpoints match well with the observed hot flaring loops and the flare ribbons, respectively, suggesting that the model has successfully "reproduced" the macroscopic magnetic process of the flare. In particular, with the simulation, we explained why this event is a confined eruption—the consequence of the reconnection is a shared arcade instead of a newly formed flux rope. We also found a much weaker magnetic implosion effect compared to many other X-class flares.

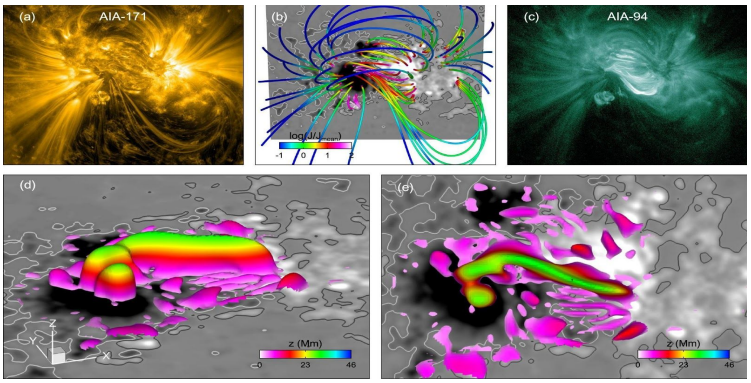


*Fig. 2. — AIA images and the simulated AR 12192 at 00:00 UT 2014 Oct 23 (i.e., simulation time t = 0). (a) AIA 171 Å image. (b) Selected magnetic field lines of the MHD simulations. The background shows map of photospheric $B_z$ (saturated at ±1000 G). Contour lines (black and white) are also shown for ±100 G. The color of the plotted field lines denotes the strength of the associated electric current density J (scaled by the mean value J of the entire model volume). (c) AIA 94 Å image. (d) The side view of the volume with the current density higher than 20 times the mean value. The color denotes the height z from the bottom boundary. (e) The top view of the same current volume shown in (c). Contour lines (black and white) are also shown for ±100 G.*

**Multi-wavelength observations of a flux rope formation by series of magnetic reconnection in the chromosphere**, *Kumar, P., Yurchyshyn, V., Cho, K.S., Wang, H.,* 2017, A&A, 603, id.A36.

Using data from the 1.6 m New Solar Telescope (NST) operating at the Big Bear Solar Observatory (BBSO), we report direct evidence of merging and reconnection of cool Hα loops in the chromosphere during two homologous flares (B and C class) caused by a shearing motion at the footpoints of two loops. The reconnection between these loops caused the formation of an unstable flux rope that showed counterclockwise rotation. To the best of our knowledge, such a clear interaction of chromospheric loops along with rapid flux cancellation has not been reported before. These high-resolution observations suggest the formation of a small flux rope by a series of magnetic reconnection within chromospheric loops that are associated with very rapid flux cancellation.

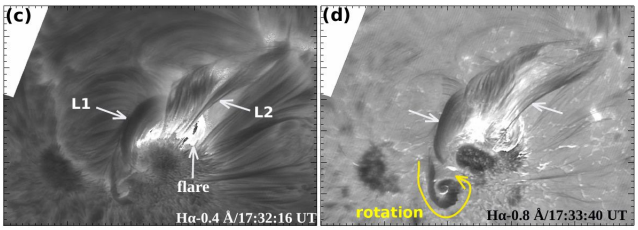


*Fig. 3. — NST Hα-0.8 Å and Hα-0.4 Å images showing the interaction of two loop system (L1 and L2) and associated C-class flare. The size of each image is 50″×35″. Each division on the x- and y axes is equal to*

*1". The coalescence of loops (L1 and L2) and formation of a resulting flux rope is shown in panel d)*

**Formation and Eruption of a Small Flux Rope in the Chromosphere Observed by NST, IRIS, and SDO** by *P. Kumar, V. Yurchyshyn, H. Wang, & K.S. Cho, 2015,* Astrophys. J., 809/1, article id. 83

Using high-resolution NST images we report direct evidence of chromospheric reconnection at the polarity inversion line between two small opposite polarity sunspots. Small jet-like structures (with velocities of 20-55 km/s) were observed at the reconnection site before the onset of the first M1.0 flare. The slow rise of untwisting jets was followed by the onset of cool plasma inflow (10 km/s) at the reconnection site, causing the onset of a two-ribbon flare. The reconnection between two sheared J-shaped cool Hα loops causes the formation of a small twisted (S-shaped) flux rope in the chromosphere. In addition, HMI magnetograms show the flux cancellation (both positive and negative) during the first M1.0 flare. The emergence of negative flux and the cancellation of positive flux (with shear flows) continue until the successful eruption of the flux rope. The newly formed chromospheric flux rope becomes unstable and rises slowly with a speed of 108 km/s during a second C8.5 flare that occurred after 3 hr of the first M1.0 flare. The flux rope was destroyed by repeated magnetic reconnection induced by its interaction with the ambient field (fan-spine topology) and looks like an untwisting surge (170 km/s) in the coronal images recorded by SDO/AIA instrument. These observations suggest the formation of a chromospheric flux rope (by magnetic reconnection associated with flux cancellation) during the first M1.0 flare and its subsequent eruption/disruption during the second C8.5 flare.

**Multiwavelength Observations of a Slow-rise, Multistep X1.6 Flare and the Associated Eruption**, *Yurchyshyn, V., Kumar, P., Cho, K.-S., Lim, E.-K., Abramenko, V. I.*, 2015, Astrophys. J., 812/2, article.id. 172

Using multiwavelength observations, we studied a slow-rise, multistep X1.6 flare that began on 2014 November 7 as a localized eruption of core fields inside a δ-sunspot and later engulfed the entire active region (AR). This flare event was associated with formation of two systems of post-eruption arcades (PEAs) and several J-shaped flare ribbons showing extremely fine details, irreversible changes in the photospheric magnetic fields, and it was accompanied by a fast and wide coronal mass ejection. Data from the Solar Dynamics Observatory and IRIS spacecraft, along with the ground-based data from NST, present evidence that (i) the flare and the eruption were directly triggered by a flux emergence that occurred inside a δ-sunspot at the boundary between two umbrae (Figure 1); (ii) this event represented an example of the formation of an unstable flux rope observed only in hot AIA channels (131 and 94 Å) and LASCO C2 coronagraph images; (iii) the global PEA spanned the entire AR and was due to global-scale reconnection occurring at heights of about one solar radius, indicating the global spatial and temporal scale of the eruption.

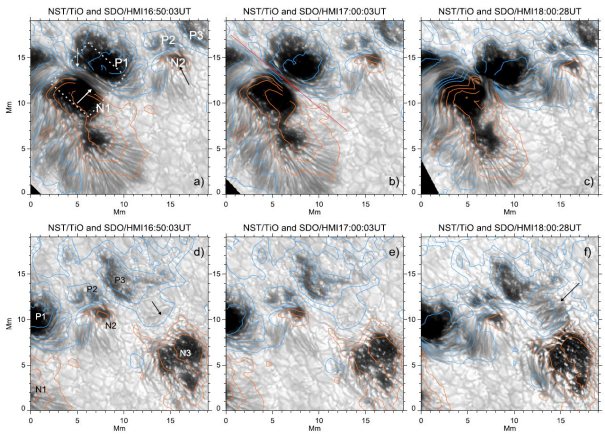


*Fig. 6. — NST/TiO photospheric images overplotted with contours of HMI vertical magnetic fields. Positive (blue) and negative (red) contours are drawn at ±200, ±500, ±800, and ±1100 G levels. The dotted box in panel (a) encloses the area used to monitor magnetic flux variations. Letters N and P mark positive and negative polarity pores. The upper panels show evolution of a δ-sunspot, as well as penumbral filaments separating them. The lower panels show the appearance of an "orphan" penumbra in the photosphere under the*

*filament (black arrows in panels (d) and (f)).*

**Observations of a Series of Flares and Associated Jet-like Eruptions Driven by the Emergence of Twisted Magnetic Fields** by *Lim, Eun-Kyung; Yurchyshyn, Vasyl; Park, Sung-Hong; Kim, Sujin; Cho, Kyung-Suk; Kumar, Pankaj; Chae, Jongchul; Yang, Heesu; Cho, Kyuhyoun; Song, Donguk; Kim, YeonHan*, 2016, Astrophys. J., 817/1, article.id. 39

We studied temporal changes of morphological and magnetic properties of a succession of four confined flares followed by an eruptive flare using the high-resolution NST data, Helioseismic and Magnetic Imager (HMI) magnetograms, and Atmospheric Image Assembly (AIA) EUV images provided by the Solar Dynamics Observatory (SDO). Analysis of NST Halpha and the SDO/AIA 304 Å images allowed us to conclude that each of the flares developed a jet structure that evolved in a manner similar to evolution of the blowout jet: (1) an inverted-Y-shaped jet appeared and drifted away from its initial position; (2) jets formed a curtain-like structure that consisted of many fine threads accompanied by subsequent brightenings near the footpoints of the fine threads; and finally, (3) the jet showed a twisted structure visible near the flare maximum. Analysis of the HMI data showed that both the negative magnetic flux and the magnetic helicity have been gradually increasing in the positive-polarity region, indicating the continuous injection of magnetic twist before and during the series of flares. Based on these results, we suggest that the continuous emergence of twisted magnetic flux played an important role in producing successive flares and developing a series of blowout jets. The newly emerging flux carried enough of magnetic twist required to power two moderate sized eruptions.

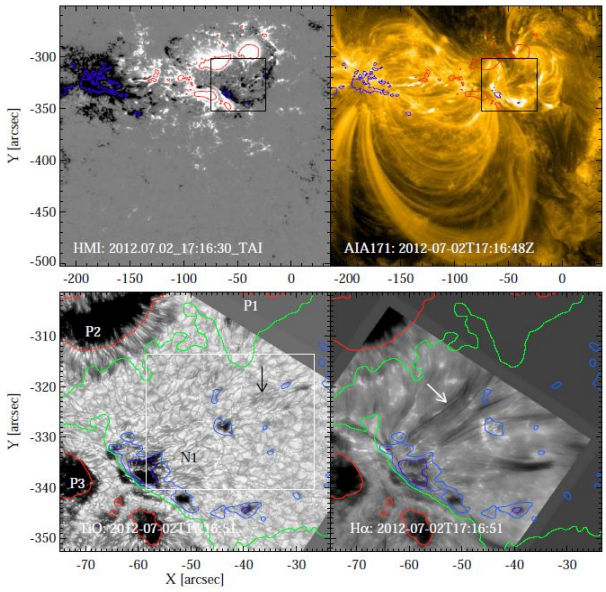


*Fig. 7.— Active region overview just before the C3.7 flare onset. SDO/HMI (upper-left) and AIA 171 °A (upper-right) images show the entire active region. NST/TiO (lower-left) and H-alpha (lower-right) data have the same field of view (FOV) as the black squares in the top panels. Contours with purple, blue and red colors represent the longitudinal magnetic field strength of [−1000,−500, 1000 G], respectively. The polarity inversion line (PIL) is over-plotted on the NST data as a green color curve. The positive sunspots are referred as a letter 'P' and the negative as 'N'.*

**Prediction of solar cycle 25: a non-linear approach**, Sarp, V., Kilcik, A., Yurchyshyn, V., Rozelot, J.P., Ozguc, A., 2018, MNRAS, 481, 2981

Predicting the solar activity is an important task for space weather and solar physics. There are various approaches to predict the solar activity and these predictions are used in various areas such as planning space missions, approximating the mechanism of solar dynamo, etc. In this paper, a non-linear prediction algorithm based on delay-time and phase space reconstruction is used to forecast the maximum of Solar Cycle 25. Apart from embedding dimension and delay-time which are the key parameters of such methods, we further found a new parameter (starting point) that should be taken into account to get better solar cycle predictions. This method was tested on last five solar cycles and the results are quite acceptable. We predicted that the maximum of Solar Cycle 25 will be at the year 2023.2 ± 1.1 with a peak sunspot number of 154 ± 12. Our results are compared with other available predictions.

**The evolution of flaring and non-flaring active regions,** Kilcik, A., Yurchyshyn, V., Sahin, S., Sarp, V., Obridko, V., Ozguc, A., Rozelot, J.P., 2018, MNRAS, 477, 293

According to the modified Zurich classification, sunspot groups are classified into seven different classes (A, B, C, D, E, F and H) based on their morphology and evolution. In this classification, classes A and B, which are small groups, describe the beginning of sunspot evolution, while classes D, E and F describe the large and evolved groups. Class C describes the middle phase of sunspot evolution and the class H describes the end of sunspot evolution. Here, we compare the lifetime and temporal evolution of flaring and non-flaring active regions (ARs), and the flaring effect on ARs in these groups in detail for the last two solar cycles (1996 through 2016). Our main findings are as follows: (i) Flaring sunspot groups have longer lifetimes than non-flaring ones. (ii) Most of the class A, B and C flaring ARs rapidly evolve to higher classes, while this is not applicable for non-flaring ARs. More than 50 per cent of the flaring A, B and C groups changed morphologically, while the remaining D, E, F and H groups did not change remarkably after the flare activity. (iii) 75% of all flaring sunspot groups are large and complex. (iv) There is a significant increase in the sunspot group area in classes A, B, C, D and H after flaring activity. In contrast, the sunspot group area of classes E and F decreased. The sunspot counts of classes D, E and F decreased as well, while classes A, B, C and H showed an increase.

**Signature of a possible relationship between the maximum CME speed index and the critical frequencies of the F1 and F2 ionospheric layers: Data analysis for a mid-latitude ionospheric station during the solar cycles 23 and 24**, Kilcik, A., Ozguc, A., Yiğit, E., Yurchyshyn V., Donmez, B., 2018, J. Atm. Sol-Ter. Phys., 171, 131

We analyze temporal variations of two solar indices, the monthly mean Maximum CME Speed Index (MCMESI) and the International Sunspot Number (ISSN) as well as the monthly median ionospheric critical frequencies (foF1, and foF2) for the time period of 1996-2013, which covers the entire solar cycle 23 and the ascending branch of the cycle 24. We found that the maximum of foF1 and foF2 occurred respectively during the first and second maximum of the ISSN solar activity index in the solar cycle 23. We compared these data sets by using the cross-correlation and hysteresis analysis and found that both foF1 and foF2 show higher correlation with ISSN than the MCMESI during the investigated time period, but when significance levels are considered correlation coefficients between the same indices become comparable. Cross-correlation analysis showed that the agreement between these data sets (solar indices and ionospheric critical frequencies) is better pronounced during the ascending phases of solar cycles, while they display significant deviations during the descending phase. We conclude that there exists a signature of a possible relationship between MCMESI and foF1 and foF2, which means that MCMESI could be used as a possible indicator of solar and geomagnetic activity, even though other investigations are needed.

**Temporal and Periodic Variations of Sunspot Counts in Flaring and Non-Flaring Active Regions**, Kilcik, A., Yurchyshyn, V., Donmez, B., Obridko, V. N., Ozguc, A., Rozelot, J.P., 2018, Sol. Phys., 293, 63

We analyzed temporal and periodic variations of sunspot counts (SSCs) in flaring (C-, M-, or X-class flares), and non-flaring active regions (ARs) for nearly three solar cycles (1986 through 2016). Our main findings are as follows: i) temporal variations of monthly means of the daily total SSCs in flaring and non-flaring ARs behave differently during a solar cycle and the behavior varies from one cycle to another; during Solar Cycle 23 temporal SSC profiles of non-flaring ARs are wider than those of flaring ARs,

while they are almost the same during Solar Cycle 22 and the current Cycle 24. The SSC profiles show a multi-peak structure and the second peak of flaring ARs dominates the current Cycle 24, while the difference between peaks is less pronounced during Solar Cycles 22 and 23. The first and second SSC peaks of non-flaring ARs have comparable magnitude in the current solar cycle, while the first peak is nearly absent in the case of the flaring ARs of the same cycle. ii) Periodic variations observed in the SSCs profiles of flaring and non-flaring ARs derived from the multi-taper method (MTM) spectrum and wavelet scalograms are quite different as well, and they vary from one solar cycle to another. The largest detected period in flaring ARs is 113± 1.6 days while we detected much longer periodicities (327± 13, 312 ± 11, and 256± 8 days) in the non-flaring AR profiles. No meaningful periodicities were detected in the MTM spectrum of flaring ARs exceeding 55± 0.7 days during Solar Cycles 22 and 24, while a 113± 1.3 days period was detected in flaring ARs of Solar Cycle 23. For the non-flaring ARs the largest detected period was only 31± 0.2 days for Cycle 22 and 72± 1.3 days for the current Cycle 24, while the largest measured period was 327± 13 days during Solar Cycle 23.

**Contribution to the Solar Mean Magnetic Field from Different Solar Regions,** Kutsenko, A.S., Abramenko, V. I., and Yurchyshyn, V. B., 2017, Sol. Phys., 292, 121

Using observations of solar magnetic fields with the Helioseismic and Magnetic Imager (HMI) on board the Solar Dynamics Observatory (SDO) we studied contribution of weak ($B^W$), intermediate ($B^I$), and strong ($B^S$) fields into the total SMMF. We found that i) when the threshold level of 30 Mx $cm^{-2}$ is applied, the $B^I$ and $B^S$ components together contribute from 65% to 95% of the SMMF, while the fraction of the occupied area varies in a range of 2 - 6% of the disk area; ii) as the threshold magnitude is lowered to 6 Mx $cm^{-2}$, the contribution from $B^I$+$B^S$ grows to 98%, and the fraction of the occupied area reaches a value of about 40% of the solar disk. In summary, we found that regardless of the threshold level, only a small part of the solar disk area contributes to the SMMF. This means that the photospheric magnetic structure is an intermittent inherently porous medium, resembling a percolation cluster. These findings suggest that the long-standing concept that continuous vast unipolar areas on the solar surface are the source of the SMMF may need to be reconsidered.

**Impact of the Icme-Earth Geometry on the Strength of the Associated Geomagnetic Storm: The September 2014 and March 2015 Events,** *Cho, K.-S., Marubashi, K., Kim, R.-S., Park, S.-H., Lim, E.-K., Kim, S.-J., Kumar, P., Yurchyshyn, V., Moon, Y.-J., Lee, J.-O.***,** 2017, J. Korea Astron. Soc., 50, 29-39

We investigated two abnormal CME-Storm pairs that occurred on 2014 September 10 - 12 and 2015 March 15 - 17, respectively. The first one was a moderate geomagnetic storm (Dst_min= -75 nT) driven by the X1.6 high speed flare-associated CME (1267 km/s) in AR 12158 (N14E02) near solar disk center. The other was a very intense geomagnetic storm (Dst_min= -223 nT) caused by a CME with speed (719 km/ s) and associated with a filament eruption accompanied by a weak flare (C9.1) in AR 12297 (S17W38). Both CMEs have large direction parameters facing the Earth and southward magnetic field orientation in their solar source region. In this study, we inspected the structure of Interplanetary Flux Ropes (IFRs) at the Earth estimated by using the torus fitting technique assuming self-similar expansion. As results, we find that the moderate storm on 2014 September 12 was caused by small-scale southward magnetic fields in the sheath region ahead of the IFR. The Earth traversed the portion of the IFR where only the northward fields are observed. Meanwhile, in case of the 2015 March 17 storm, our IFR analysis revealed that the Earth passed the very portion where only the southward magnetic fields are observed throughout the passage. The resultant southward magnetic field with long-duration is the main cause of

the intense storm. We suggest that 3D magnetic field geometry of an IFR at the IFR-Earth encounter is important and the strength of a geomagnetic storm is strongly affected by the relative location of the Earth with respect to the IFR structure.

**Analysis of the Flux Growth Rate in Emerging Active Regions on the Sun**, *Abramenko, V. I. , Kutsenko, A. S., Tikhonova, O. I., & Yurchyshyn, V. B.,* 2017, Sol. Phys., 292,article id.48

We studied the emergence process of 42 active regions (ARs) by analyzing the time derivative, R(t), of the total unsigned flux. Line-of-sight magnetograms acquired by the Helioseismic and Magnetic Imager (HMI) onboard the Solar Dynamics Observatory (SDO) were used. A continuous piecewise linear fitting to the R(t)-profile was applied to detect an interval, $\Delta t_2$, of nearly constant R(t) covering one or several local maxima. Out of 42 ARs in our initial list, 36 events were successfully fitted, and they form two subsets (with a small overlap of eight events): the ARs with a short (<13 hours) interval $\Delta t_2$ and a high (>0.024 hour$^{-1}$) normalized flux emergence rate, formed the "rapid" emergence event subset. The second subset consists of "gradual" emergence events, and it is characterized by a long (>13 hours) interval $\Delta t_2$ and a low flux emergence rate. Events from different subsets do not overlap, and each subset displays an individual power law. The power-law index derived from the entire ensemble of 36 events is $0.69 \pm 0.10$. The rapid emergence is consistent with a two-step emergence process of a single twisted flux tube. The gradual emergence is possibly related to a consecutive rising of several flux tubes emerging at nearly the same location in the photosphere.

**Solar and Geomagnetic Activity Relation for the Last two Solar Cycles**, *Kilcik, A., Yigit, E., Yurchyshyn, V., Ozguc, A., & Rozelot, J.P.,* 2017, Sun & Geosphere, 12, 1, 31-39

The long-term relationship between solar (sunspot counts in different Zurich sunspot groups, International Sunspot Number (ISSN), solar wind, and X-Ray solar flare index and geomagnetic indices (Ap and Dst) is investigated. Data sets used in this study cover a time period from January 1996 to March 2014. Our main findings are as follows: 1) The best correlation between the sunspot counts and the Ap index are obtained for the large group time series, while the other categories exhibited lower (final and medium) or no correlation at all (small). It is interesting to note that Ap index is delayed by about 13 months relatively to all sunspot count series and ISSN data. 2) The best correlation between the sunspot counts and the Dst index was as well obtained for the large AR time series. The Dst index delays with respect to the large group by about 2 months. 3) The highest correlation between the solar and geomagnetic indices were obtained between the solar wind speed and Ap and Dst indices with zero time delays ($r = 0.76$, $r = 0.52$, respectively). 4) The correlation coefficients between the geomagnetic indices (Ap, Dst) and X-Ray solar flare index ($r = 0.59$, $r = -0.48$, respectively) are a little higher than the correlation coefficients between these geomagnetic indices and ISSN ($r = 0.57$, $r = -0.43$, respectively). 5) The magnitude of all solar and geomagnetic indices (except the solar wind speed) has significantly decreased during the current solar cycle as compared to the same phase of the previous cycle.

**Flare-production potential associated with different sunspot groups**, *Eren, S., Kilcik, A., Atay, T., Miteva, R., Yurchyshyn, V., Rozelot, J. P., Ozguc, A.*, 2017, MNRAS, 465, 68-75

In this study, we analysed different types (C, M, and X classes) of X-ray solar flares occurring in sunspot groups. The data cover 1996-2014 time interval, and a total of 4262 active regions (ARs) were included in the data set. We defined the solar-flare-production potential as the ratio of the total number of flares observed in a sunspot group to the total number of the same-class sunspot groups. Our main findings are as follows: (1) large and complex sunspot groups (D+E+F) have the flare-production potential about eight

times higher than the small and simple (A+B+C+H) ARs; (2) 79 per cent of all flares were produced by the large and complex sunspot groups, while only 21 per cent of flares were produced by the small groups; (3) the largest and the most complex F-class (very large and very complex) sunspot groups exhibit the highest flare-production potential (2.16 flare per sunspot group), while the smallest and the least complex A class sunspot groups show the lowest (0.05 flare per group) flare-production potential; (4) temporal variation of sunspot counts, sunspot group areas, and the total number of flares (including C flares) showed similar time profiles during both cycles with multiple peaks; (5) the mean area of ARs very well describes the flare-production potential of each group with the regression coefficient of $R^2$ = 0.99.